PERGAMON International Journal of Mechanical Sciences 41 (1999) 1301–1322

International Journal of MECHANICAL SCIENCES

Theoretical and experimental investigations on the spinning BTA deep-hole drill shafts containing fluids and subject to axial forces

Yuh-Lin Perng, Jih-Hua Chin*

Department of Mechanical Engineering, National Chiao Tung University, Ta Hsuch Road, Hsinchu, Taiwan, Republic of China

Received 14 April 1997; received in revised form 25 August 1998

Abstract

The object of this investigation is to develop equations of motion and analyze the eigenproperties of spinning boring trepanning association (BTA) deep-hole drill shafts containing flowing fluid and subject to compressive axial force. The energy formulations are based on a coordinate system attached to the spinning shaft (floating coordinate system), and the equations of motion were derived using Hamilton's principle. This problem was studied for two different models: a Timoshenko beam model (which includes shear deformation, rotatory inertia moment, and gyroscopic moment effects) and a Euler–Bernoulli beam model. Galerkin's method was used to obtain solutions of the dynamic system. And two kinds of experimental test were performed to investigate the eigenproperties of spinning BTA deep-hole drill shafts: impulsive testing for non-spinning tool shafts, and random-input excitation testing for spinning tool shafts. Experimental results are also compared with simulation results.

Keywords: Eigenproperties; Deep-hole drilling; Timoshenko beam; Euler–Bernoulli beam

Notation

x, y	transverse displacement in the x_1 and x_2 directions
w	axial displacement in the x_3 direction
$\tilde{u}$, $\tilde{\psi}$	complex transverse displacement and rotational angle
ds_1, ds_2	shortening displacement due to compressive axial force P
A, A_f	cross-sectional area of drill shaft and flowing fluid, respectively

* Corresponding author.

0020-7403/99/$ - see front matter
PII: S0020-7403(98)00091-5

ρ, ρ_f	mass density of drill shaft and fluid flow, respectively
I	moment of inertia of area A
I_f	moment of inertia of area A_f
J_P	polar mass moment of inertia of area A per unit length
J_{Pf}	polar mass moment of inertia of area A_f per unit length
U	flowing fluid velocity in axial direction
U_{cr}	maximum velocity of flowing fluid
U_c	critical fluid flow velocity
$\bar{\Gamma}$	non-dimensional fluid flow velocity
Ω	spinning speed of drill shaft
$\bar{\Im}$	non-dimensional spinning speed
M	mass of the fluid per unit length ($M = \rho_f A_f$)
α, β	rotational angle in the x_1–x_3 and x_2–x_3 plane, respectively
γ_1, γ_2	shear angle
l	length of drill shaft
E	Young's modulus of drill shaft
G	shearing modulus of drill shaft
k	Timoshenko shear coefficient
P	compressive axial force
P_{cr}	Euler critical buckling load ($= \pi^2 EI/l^2$)
N_c	critical axial loading
$\bar{\Re}$	non-dimensional compressive axial force
σ_{ij}	stress components
ε_{ij}	strain components
$q_i(\bar{t})$	generalized time-dependent coordinates
$\phi_i(\zeta)$	comparison function
λ_i	non-dimensional eigenvalues of $\phi_i(\zeta)$
μ	complex eigenvalue $\mu(= \tau + \mathrm{i}\omega)$
τ	real part of complex eigenvalue μ
ϖ	natural frequency of the drill shaft
ϖ_n	nth mode natural frequency
ω_{10}	first mode "at-rest" natural frequency
$\bar{\varpi}$	non-dimensional natural frequency parameter
$\bar{I}$	identity matrix
$\bar{0}$	zero matrix
n	truncated number of Galerkin's method
$M_{1,2}$	bending moment
$V_{1,2}$	shear force
p	fluid pressure
q	shear stress on the internal surface of the drill tube

1. Introduction

Deep-hole drilling is defined as the ratio of a required hole depth to its diameter being greater than 10. Because the shafts used for this purpose are extraordinarily long compared with their diameter, the dynamics of drill shaft become important to cutting quality with respect to hole

tolerances, roundness, and straightness. Therefore, it is necessary to examine the eigen- as well as the dynamic properties of drill shafts.

1.1. Purpose of this study

Deep-hole drilling systems consist of long drill tubes with fluid through the bores of tubes and drilling heads under high pressure. There are two types of deep-hole drilling, one uses a spinning drill and a stationary workpiece, the other uses a spinning workpiece and a stationary drill.

Most researchers have studied how cutting quality is affected by cutting conditions, such as, tool material, cutting forces, action of burnishing pads, drill wear, and cutting tool head design. The behaviors of BTA deep-hole drill shafts have rarely been discussed in recent years. Chin et al. [1, 2] recently attempted to predict the behavior of a non-spinning BTA deep-hole drill shaft with (and without) flowing fluid, but spinning tool shafts have remained unstudied.

Since the characteristics of long spinning tubes with fluid flowing through them and subject to axial compressive forces have rarely been discussed in the literature, this paper explores the dynamic responses of spinning BTA drill shafts carrying fluid and subject to compressive forces in the axial direction. We formulate the energy in terms of a floating coordinate system and derive equations of motion based on Timoshenko and Euler–Bernoulli beam theories using Hamilton's principle. The dynamic-system solutions were found by Galerkin's method. Simulation and experimental results are compared and discussed in the paper.

1.2. Literature review

Chin et al. [3, 4] proposed a mathematical model for simulating chip flowing in gun drilling and experimentally monitored the pressure of the chip-carrying fluid using piezoelectric transducers. Later, Chin and Lin [5] set up a theoretical model treating the tool shaft as a second-order lumped mass system in order to investigate the stability of the gundrill cutting process. Sakuma et al. [6] showed that the effects of tool-head vibration (one kind of self-excited vibration) formed polygonal holes. He proposed a simple formula that described the mechanism by which multi-corner holes were formed but did not study the bending vibration of the drill shaft carrying fluid.

The studies mentioned below proposed theories concerning the dynamic responses of spinning or non-spinning shafts with various considerations such as subject to a axial force, shear deformation, rotatory inertia moment, gyroscopic moment, etc. Huang [7] constructed a mathematical model of a non-spinning beam with classical boundary conditions to estimate natural frequencies and normal modes using Timoshenko beam theory. Thirty years later, Zu and Han [8] extended this study to derive the exact natural frequencies and normal modes of a spinning Timoshenko beam with general boundary conditions. Eshleman and Eubanks [9] investigated the effect of axial torque on the critical speeds of a continuous rotor whose motion was described by a set of partial differential equations that included consideration of the effects of transverse shear, rotatory inertia, and gyroscopic moments. Nelson [10] used the finite-element method to analyze the eigenquantities and critical speeds of a finite spinning Timoshenko beam element. The effects of rotatory inertia, gyroscopic moments, axial force, and internal damping were also considered, but shear deformation was not. Bauer [11] published a thorough treatment of a spinning shaft under all possible combinations of classical boundary conditions using Euler beam theory. Lee et al. [12]

employed the modal analysis technique to study the forced responses of an undamped distributed-parameter spinning shaft, including its rotatory inertia and gyroscopic effects, and allowing for various boundary conditions. The non-self-adjoint eigenvalue problem was also considered in his study using the modal analysis technique. Sato [13] examined the equations governing vibration and stability of a Timoshenko beam from the stand point of Hamilton's principle. Choi et al. [14] presented consistent derivation of a set of equations of motion describing the flexural and torsional vibrations of a straight spinning shaft subject to axial loading. Farchaly and Shebl [15] derived the exact mode shapes and natural frequencies of an axially loaded Timoshenko beam carrying elastically supported end masses.

A study of a pipe containing flowing fluid was published by Housner and Calif [16] in 1952. Paidoussis et al. [17, 18] extended this study to cover the dynamic stability of pipes conveying fluid at constant and pulsating flow velocities. Weaver and Unny [19] showed that the dynamic stability of pipes conveying fluid is stimulated by transverse vibration based on observation of the Trans-Arabian pipeline. Blevins [20] suggested that the planar lateral motions of pipes carrying fluid at constant velocities, and critical flow velocities are due to buckling and fluttering of the pipe.

Since BTA deep-hole drills combine beams, pipes, and pressurized internal fluid flows, none of the available equations of motion properly describe the behavior in particularly when they are also subject to a compressive forces in the axial direction. In this paper, we attempt to establish equations of motion for a spinning BTA deep-hole drill shaft containing flowing fluid and subject to axial loading. The proposed equations were solved for lateral motions and the results were verified by experiment.

2. Equations of motion

The differential equations governing the transverse dynamic motion of a spinning drill shaft containing flowing fluid and subject to a compressive axial force are derived in this section. This problem is studied using two models: a Timoshenko beam model (which includes shear deformations, rotatory inertia moment, and gyroscopic moment effects) and a Euler–Bernoulli beam model. The basic assumptions about the drill shaft are as follows: (1) The drill shaft has a uniform cross section along its length. (2) The plane sections is normal to the centroidal line of the drill shaft in its undeformed state and Poisson effects are ignored, i.e., stresses through the thickness of drill shaft are ignored. (3) The drill shaft is balanced, i.e., at every cross section, the mass center coincides with the geometric center. (4) A compressive axial force P of constant magnitude is applied at the ends. (5) Axial deformations due to the compressive axial force P are considered. (6) The drill shaft is spinning at a constant angular velocity Ω about its longitudinal axis. (7) The fluid flow velocity is constant in the axial direction. (8) The drill shaft material is assumed to be isotropic and homogeneous.

The inertial coordinate system $OX_1X_2X_3$, and the floating coordinate system $ox_1x_2x_3$ used in formulating the equations of motion are shown in Fig. 1. The $ox_1x_2x_3$ system rotates at a constant speed of Ω, and is attached to drill shaft at its centroid. According to the Timoshenko beam theory, the deformed state can be expressed as two centerline elastic displacements of the drill shaft x, and y, in the x_1 and x_2 directions, and the small rotations α and β about the x_2 and x_1 axes. A small free-body diagram element of a drill shaft of length ds, and a corresponding enclosed fluid component of volume dV are shown in Fig. 2.

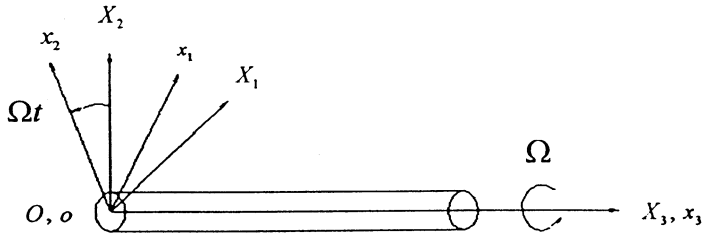

Fig. 1. The inertial and rotating coordinate system of the drill shaft.

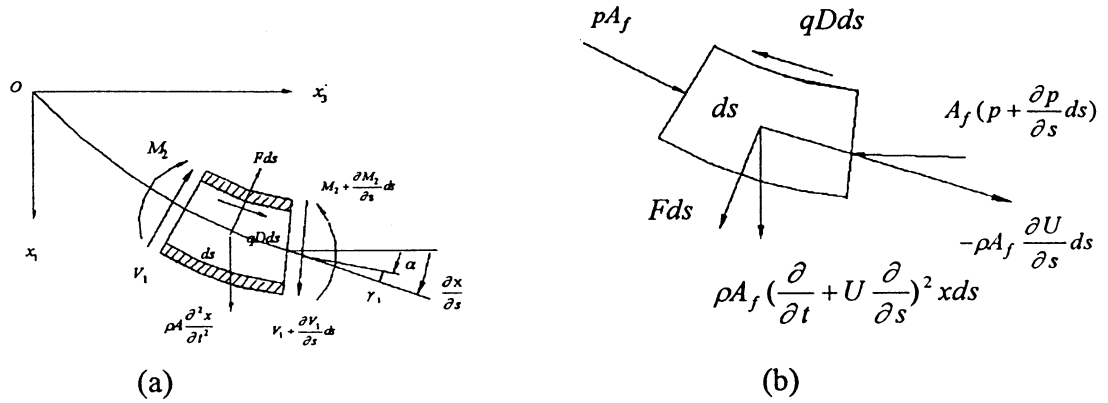

Fig. 2. Free-body diagram of a drill shaft and a controlled volume of enclosed fluid on the x_1–x_3 plane: (a) Tool shaft element; (b) Fluid element.

We derive the differential equations of motion of a spinning drill shaft using Hamilton's principle, as given by

$$\delta \int_{t_1}^{t_2} (T - V + W)\,\mathrm{d}t = 0, \tag{1}$$

where T and V are kinetic and potential energies and δW is the virtual work done by the compressive axial force P. All of quantities below are specified on the floating coordinate system.

The kinetic energy of the drill shaft due to translation and rotation can be expressed as

$$T_s = \frac{1}{2}\int_0^l \{\rho A[\dot{x}^2 + \dot{y}^2 + 2\Omega(x\dot{y} - \dot{x}y) + \Omega^2(x^2 + y^2)] + \rho I[\dot{\alpha}^2 + \dot{\beta}^2 + \Omega^2(\alpha^2 + \beta^2)]\}\,\mathrm{d}s, \tag{2}$$

where ρ is the mass density, A is the cross-sectional area, I is the second moment of area, and Ω is the spinning speed of drill shaft.

The kinetic energy of the flowing fluid [19] is given by

$$T_f = \frac{1}{2}\int_0^l \{M[U^2 + (\dot{x} + Ux_s)^2 + (\dot{y} + Uy_s)^2 + 2\Omega x(\dot{y} + Uy_s) - 2\Omega y(\dot{x} + Ux_s) + \Omega^2(x^2 + y^2)] + \rho_f I_f[\dot{\alpha}^2 + \dot{\beta}^2 + \Omega^2(\alpha^2 + \beta^2)]\}\,\mathrm{d}s. \tag{3}$$

The parameter M is the mass of fluid per unit length, ρ_f is the mass density of the flowing fluid, A_f is the cross section of the flowing fluid in the drill tube, U is the fluid flow velocity in the axial direction, I_f is the second moment of area A_f.

The total kinetic energy is the sum of the kinetic energy of the drill shaft and the flowing fluid. It is written as

$$T = T_s + T_f. \tag{4}$$

The potential energy of the drill shaft due to bending and shear deformations is expressed as

$$V = \frac{1}{2}\int_v \sigma_{ij}\varepsilon_{ij}\,\mathrm{d}v$$

$$= \frac{1}{2}\int_0^l \{EI(\alpha_s^2 + \beta_s^2) + kAG[(x_s - \alpha)^2 + (y_s - \beta)^2]\}\,\mathrm{d}s, \tag{5}$$

where σ_{ij} and ε_{ij} are listed in Appendix A.

The virtual work due to the compressive axial force of a Timosheko beam, which includes the effects of shear deformation and bending deformation is

$$\delta W_P = \delta\int_0^l P(\mathrm{d}s_1 + \mathrm{d}s_2), \tag{6}$$

where $\mathrm{d}s_1$ and $\mathrm{d}s_2$ are geometric shortening at $s = l$ on the x_1–x_3 and x_2–x_3 planes, respectively. The following approximate relationships hold for a Timoshenko beam model.

$$\mathrm{d}s_1 \cong -\tfrac{1}{2}(x_s^2 - \gamma_1^2)\,\mathrm{d}s, \tag{7}$$

$$\mathrm{d}s_2 \cong -\tfrac{1}{2}(y_s^2 - \gamma_2^2)\,\mathrm{d}s, \tag{8}$$

where γ_1 and γ_2 are shear angles. The second terms in Eqs. (7) and (8) are ignored for the Euler–Bernoulli beam model. Applying Hamilton's principle, the equations of motion for a spinning drill shaft containing flowing fluid and subject to a compressive axial force expressed in the floating coordinate system can be obtained from

$$(\rho A + M)\ddot{x} + 2MU\dot{x}_s - 2\Omega(\rho A + M)\dot{y} + M\dot{U}\dot{x}_s - 2MU\Omega y_s$$
$$- \Omega^2(\rho A + M)x + (kAG + P)\alpha_s + (MU^2 - kAG)x_{ss} = 0, \tag{9}$$

$$(\rho A + M)\ddot{y} + 2MU\dot{y}_s + 2\Omega(\rho A + M)\dot{x} + M\dot{U}\dot{y}_s + 2MU\Omega x_s - \Omega^2(\rho A + M)y$$
$$+ (kAG + P)\beta_s + (MU^2 - kAG)y_{ss} = 0, \tag{10}$$

$$(\rho I + \rho_f I_f)\ddot{\alpha} - EI\alpha_{ss} - (kAG + P)(x_s - \alpha) + \Omega^2(\rho I + \rho_f I_f)\alpha = 0, \tag{11}$$

$$(\rho I + \rho_f I_f)\ddot{\beta} - EI\beta_{ss} - (kAG + P)(y_s - \beta) + \Omega^2(\rho I + \rho_f I_f)\beta = 0, \tag{12}$$

where the subscript denotes partial differentiation with respect to s in the x_3 direction.

If fluid flow M is ignored for a non-spinning drill shaft with two degrees of freedom in Eqs. (9)–(12), they are the same as the equations in [13, 15]. If fluid flow M and compressive axial force P are both ignored in Eqs. (9)–(12), they are the same as the homogeneous equations in [21]. Eqs. (9)–(12) are coupled partial differential equations. For convenience, the complex rotation and deflection are used to Eqs. (9)–(12). Let

$$\tilde{\psi} = \alpha + \mathrm{i}\beta, \tag{13}$$

$$\tilde{u} = x + \mathrm{i}y, \tag{14}$$

$$\mathrm{i} = \sqrt{-1}. \tag{15}$$

Substituting $\tilde{\psi}$ and $\tilde{u}$ into Eqs. (9)–(12), we obtain the complex-form Equations of motion as follows:

$$(\rho A + M)\ddot{\tilde{u}} + 2MU\dot{\tilde{u}}_s + \mathrm{i}2\Omega(\rho A + M)\dot{\tilde{u}} + M\dot{U}\tilde{u}_s + \mathrm{i}2MU\Omega\tilde{u}_s - \Omega^2(\rho A + M)\tilde{u} + (kAG + P)\tilde{\psi}_s + (MU^2 - kAG)\tilde{u}_{ss} = 0, \tag{16}$$

$$(\rho I + \rho_f I_f)\ddot{\tilde{\psi}} - EI\tilde{\psi}_{ss} - (kAG + P)(\tilde{u}_s - \tilde{\psi}) + \Omega^2(\rho I + \rho_f I_f)\tilde{\psi} = 0. \tag{17}$$

The equation for transverse vibration of a spinning drill shaft containing flowing fluid and subject to a compressive axial force for a Timoshenko beam model can be easily obtained from Eqs. (16) and (17):

$$\begin{aligned}
&\frac{(\rho A + M)(\rho I + \rho_f I_f)}{EI(kAG - MU^2)}\dddot{\tilde{u}} + \frac{2MU(\rho I + \rho_f I_f)}{EI(kAG - MU^2)}\ddot{\tilde{u}}_s + \mathrm{i}\frac{2\Omega(\rho A + M)(\rho I + \rho_f I_f)}{EI(kAG - MU^2)}\ddot{\tilde{u}} \\
&- \left[\frac{\rho A + M}{kAG - MU^2} + \frac{\rho I + \rho_f I_f}{EI}\right]\ddot{\tilde{u}}_{ss} + \mathrm{i}\frac{2MU\Omega(\rho I + \rho_f I_f)}{EI(kAG - MU^2)}\ddot{\tilde{u}}_s + \frac{(\rho A + M)(kAG + P)}{EI(kAG - MU^2)}\ddot{\tilde{u}} \\
&- \frac{2MU}{kAG - MU^2}\dot{\tilde{u}}_{sss} - \mathrm{i}\frac{2\Omega(\rho A + M)}{kAG - MU^2}\dot{\tilde{u}}_{ss} + \frac{2MU(KAG + P)}{EI(kAG - MU^2)}\left(\frac{\rho I + \rho_f I_f}{kAG + P}\Omega^2 + 1\right)\dot{\tilde{u}}_s \\
&+ \mathrm{i}\frac{2\Omega(\rho A + M)(KAG + P)}{EI(kAG - MU^2)}\left(\frac{\rho I + \rho_f I_f}{kAG + P}\Omega^2 + 1\right)\dot{\tilde{u}} \\
&- \frac{\Omega^2(\rho A + M)(KAG + P)}{EI(kAG - MU^2)}\left(\frac{\rho I + \rho_f I_f}{kAG + P}\Omega^2 + 1\right)\tilde{u} \\
&+ \mathrm{i}\frac{2MU\Omega(KAG + P)}{EI(kAG - MU^2)}\left(\frac{\rho I + \rho_f I_f}{kAG + P}\Omega^2 + 1\right)\tilde{u}_s + \left[\frac{\Omega^2(\rho A + M)}{kAG - MU^2}\right. \\
&- \frac{KAG + P}{EI}\left(\frac{\rho I + \rho_f I_f}{kAG + P}\Omega^2 + 1\right) \\
&\left. + \frac{(KAG + P)^2}{EI(kAG - MU^2)}\right]\tilde{u}_{ss} - \mathrm{i}\frac{2MU\Omega}{kAG - MU^2}\tilde{u}_{sss} + \tilde{u}_{ssss} = 0
\end{aligned} \tag{18}$$

If fluid flow M is ignored for a non-spinning drill shaft in Eq. (18), it is the same as the equation in [13]. Fluid flow M and compressive axial force P can be ignored for a non-spinning drill shaft in Eq. (18). Eq. (18) then becomes the same as the equation in [7].

Eq. (18) can be rendered dimensionless by using the following dimensionless parameters:

$$\eta = \frac{\tilde{u}}{l}, \quad \zeta = \frac{s}{l}, \quad \bar{t} = \frac{t}{l}\left[\frac{EI(kAG - MU^2)}{(\rho A + M)(\rho I + \rho_f I_f)}\right]^{1/4}$$

$$\bar{\Omega} = l\Omega\left[\frac{(\rho I + \rho_f I_f)^3(kAG - MU^2)}{(EI)^3(\rho A + M)}\right]^{1/4},$$

$$\bar{U} = U\left[\frac{EI(\rho A + M)^3}{(\rho I + \rho_f I_f)(kAG - MU^2)^3}\right]^{1/4},$$

$$\bar{M} = \left[\frac{EI(\rho A + M)}{(kAG - MU^2)(\rho I + \rho_f I_f)}\right]^{1/2}, \tag{19}$$

$$\bar{m} = \frac{M}{\rho A + M}, \quad \bar{P} = \frac{MU^2 + P}{kAG - MU^2},$$

$$\bar{K} = \frac{kAG + P}{EI}l^2, \quad \bar{R} = \frac{kAG + P}{kAG - MU^2},$$

which takes the following form:

$$\ddot{\dot{\eta}} + \frac{2\bar{m}\bar{U}}{\bar{M}}\dot{\dot{\eta}}_\zeta + \mathrm{i}2\bar{M}\bar{\Omega}\ddot{\eta} - \left(\bar{M} + \frac{1}{\bar{M}}\right)\ddot{\eta}_{\zeta\zeta} + \mathrm{i}2\bar{m}\bar{U}\bar{\Omega}\ddot{\eta}_\zeta + \bar{M}\bar{K}\ddot{\eta} - 2\bar{m}\bar{U}\dot{\eta}_{\zeta\zeta\zeta}$$
$$- \mathrm{i}2\bar{\Omega}\bar{M}^2\dot{\eta}_{\zeta\zeta} + 2\bar{m}\bar{U}(\bar{K} + \bar{M}\bar{\Omega}^2)\dot{\eta}_\zeta + \mathrm{i}2(\bar{K}\bar{M}^2\bar{\Omega} + \bar{M}^3\bar{\Omega}^3)\dot{\eta}$$
$$- (\bar{K}\bar{M}^3\bar{\Omega}^2 + \bar{M}^4\bar{\Omega}^4)\eta + \mathrm{i}2(\bar{m}\bar{U}\bar{K}\bar{M}\bar{\Omega} + \bar{m}\bar{U}\bar{M}^2\bar{\Omega}^3)\eta_\zeta + (\bar{M}^3\bar{\Omega}^2 - \bar{M}\bar{\Omega}^2 - \bar{K} + \bar{K}\bar{R})\eta_{\zeta\zeta}$$
$$- \mathrm{i}2\bar{m}\bar{U}\bar{M}\bar{\Omega}\eta_{\zeta\zeta\zeta} + \eta_{\zeta\zeta\zeta\zeta} = 0. \tag{20}$$

The equations of motion based on the Euler–Bernoulli beam theory for a spinning drill shaft with flowing fluid and subject to a compressive axial force can be obtained in a similar way. In Euler–Bernoulli beam theory, the effects of shear deformation, gyroscopic moment, and moment of cross-sectional rotatory inertia are ignored. Therefore, we obtain the following equation:

$$\frac{\rho A + M}{EI}\ddot{\dot{\tilde{u}}} + \mathrm{i}\frac{2\Omega(\rho A + M)}{EI}\dot{\dot{\tilde{u}}} - \frac{\Omega^2(\rho A + M)}{EI}\tilde{u}$$
$$+ \frac{2MU}{EI}\dot{\tilde{u}}_s + \mathrm{i}\frac{2MU\Omega}{EI}\tilde{u}_s + \frac{MU^2 + P}{EI}\tilde{u}_{ss} + \tilde{u}_{ssss} = 0. \tag{21}$$

If the fluid flow M and compressive axial force P are ignored for a non-spinning drill shaft in Eq. (21), it is the same as the equations in [22, 2] where the damping effect is considered in [2].

By introducing the following dimensionless terms to simplify Eq. (21):

$$\eta = \frac{\tilde{u}}{l}, \quad \zeta = \frac{s}{l}, \quad \bar{t}_E = \frac{t}{l^2}\left[\frac{EI}{\rho A + M}\right]^{1/2}$$
$$\bar{\Omega}_E = l^2\Omega\left[\frac{\rho A + M}{EI}\right]^{1/2}, \quad \bar{U}_E = lU\left[\frac{\rho A + M}{EI}\right]^{1/2} \tag{22}$$
$$\bar{m} = \frac{M}{\rho A + M}, \quad \bar{K} = \frac{MU^2 + P}{EI}l^2,$$

one gets the dimensionless equation of transverse vibration for a Euler–Bernoulli beam model:

$$\ddot{\eta} + \mathrm{i}2\bar{\Omega}_E\dot{\eta} - \bar{\Omega}_E^2\bar{m}\eta + 2\bar{m}\bar{U}_E\dot{\eta}_\zeta + \mathrm{i}2\bar{m}\bar{U}_E\bar{\Omega}_E\eta_\zeta + \bar{K}\eta_{\zeta\zeta} + \eta_{\zeta\zeta\zeta\zeta} = 0. \tag{23}$$

In this study, we formulate the equations of motion in the floating coordinate system. The mass moment of inertia remains unchanged with spinning speed.

3. Method of solution

Galerkin's method was used analytically to solve the equations of a spinning Timoshenko beam and a Euler–Bernoulli beam carrying fluid and loaded by compressive axial force. According to Galerkin's method, the quantity $\eta(\zeta, \bar{t})$ can be expressed as a product of the time-dependent generalized coordinates $q_i(\bar{t})$ and comparison functions $\phi_i(\zeta)$:

$$\eta(\zeta, \bar{t}) = \sum_{i=1}^{n} q_i(\bar{t})\phi_i(\zeta), \tag{24}$$

where $\phi_i(\zeta)$ are comparison functions that satisfy the boundary conditions at the two ends of beam. In this study, the boundary condition of the drill shaft is assumed to be clamping at one end and hinging at the other end. Thus,

$$\eta(0, \bar{t}) = 0, \quad \eta_\zeta(0, \bar{t}) = 0,$$
$$\eta(1, \bar{t}) = 0, \quad \eta_{\zeta\zeta}(1, \bar{t}) = 0. \tag{25}$$

The comparison functions $\phi_i(\zeta)$ are found to be

$$\phi_i(\zeta) = \cosh\lambda_i\zeta - \cos\lambda_i\zeta + \sigma_i(\sinh\lambda_i\zeta - \sin\lambda_i\zeta) \tag{26}$$

with

$$\sigma_i = -\frac{\cosh\lambda_i - \cos\lambda_i}{\sinh\lambda_i - \sin\lambda_i}, \tag{27}$$

where λ_i are the solutions of

$$\tanh\lambda_i = \tan\lambda_i. \tag{28}$$

The dimensionless values λ_i are listed in Table 1.

Table 1
The values of λ_i

λ_i	value of λ_i	λ_i	value of λ_i
λ_1	3.92660246	λ_6	19.63495408
λ_2	7.06858275	λ_7	22.77654674
λ_3	10.21017612	λ_8	25.91813939
λ_4	13.35176878	λ_9	29.05973205
λ_5	16.49336143	λ_{10}	32.20132470

Substituting Eq. (24) into Eq. (20), multiplying by $\phi_j(\zeta)$, and integrating it from 0 to 1, due to the orthonormal property of the comparison functions used, the resulting dimensionless equation of motion in matrix form for a Timoshenko beam model becomes

$$\bar{A}\ddot{\chi} + \bar{B}\dot{\ddot{\chi}} + \bar{C}\ddot{\chi} + \bar{D}\dot{\chi} + \bar{E}\chi = 0, \tag{29}$$

where matrices $\bar{A}$, $\bar{B}$, $\bar{C}$, $\bar{D}$, and $\bar{E}$ are defined as

$$[\bar{A}]_{ij} = \bar{a}_{ij},$$

$$[\bar{B}]_{ij} = \frac{2\bar{m}\bar{U}}{\bar{M}}\bar{b}_{ij} + \mathrm{i}2\bar{M}\bar{\Omega}\bar{a}_{ij},$$

$$[\bar{C}]_{ij} = -\left(\bar{M} + \frac{1}{\bar{M}}\right)\bar{c}_{ij} + \mathrm{i}2\bar{m}\bar{U}\bar{\Omega}\bar{b}_{ij} + \bar{M}\bar{K}\bar{a}_{ij},$$

$$[\bar{D}]_{ij} = -2\bar{m}\bar{U}\bar{d}_{ij} - \mathrm{i}2\bar{\Omega}\bar{M}^2\bar{c}_{ij} + 2\bar{m}\bar{U}(\bar{K} + \bar{M}\bar{\Omega}^2)\bar{b}_{ij} + \mathrm{i}2(\bar{\Omega}^3\bar{M}^3 + \bar{K}\bar{\Omega}\bar{M}^2)\bar{a}_{ij},$$

$$[\bar{E}]_{ij} = \bar{e}_{ij} - \mathrm{i}2\bar{m}\bar{U}\bar{\Omega}\bar{M}\bar{d}_{ij} + (\bar{\Omega}^2\bar{M}^3 - \bar{\Omega}^2\bar{M} - \bar{K} + \bar{K}\bar{R})\bar{c}_{ij}$$
$$+ \mathrm{i}2(\bar{K}\bar{m}\bar{U}\bar{M}\bar{\Omega} + \bar{\Omega}^3\bar{m}\bar{U}\bar{M}^2)\bar{b}_{ij} - (\bar{\Omega}^4\bar{M}^4 + \bar{K}\bar{\Omega}^2\bar{M}^3)\bar{a}_{ij}$$

and

$$\bar{a}_{ij} = \int_0^1 \phi_i(\zeta)\phi_j(\zeta)\,\mathrm{d}\zeta = \begin{cases} 0, & i \neq j, \\ 1, & i = j, \end{cases}$$

$$\bar{b}_{ij} = \int_0^1 \phi_i(\zeta)\phi_{j,\zeta}(\zeta)\,\mathrm{d}\zeta = \begin{cases} \dfrac{4\lambda_i^2\lambda_j^2}{\lambda_j^4 - \lambda_i^4}[(-1)^{i+j} - 1], & i \neq j, \\ 0, & i = j, \end{cases}$$

$$\bar{c}_{ij} = \int_0^1 \phi_i(\zeta)\phi_{j,\zeta\zeta}(\zeta)\,\mathrm{d}\zeta = \begin{cases} \dfrac{4\lambda_i^2\lambda_j^2}{\lambda_j^4 - \lambda_i^4}(\lambda_j\sigma_j - \lambda_i\sigma_i)[(-1)^{i+j} + 1], & i \neq j, \\ 0, & i = j, \end{cases}$$

$$\bar{d}_{ij} = \int_0^1 \phi_i(\zeta)\phi_{j,\zeta\zeta\zeta}(\zeta)\,\mathrm{d}\zeta = \begin{cases} \dfrac{4\lambda_i^2\lambda_j^2}{\lambda_j^4 - \lambda_i^4}[\sigma_i\sigma_j - (-1)^{i+j}], & i \neq j, \\ 0, & i = j, \end{cases}$$

$$\bar{e}_{ij} = \int_0^1 \phi_i(\zeta)\phi_{j,\zeta\zeta\zeta\zeta}(\zeta)\,\mathrm{d}\zeta = \begin{cases} 0, & i \neq j, \\ \lambda_i^4, & i = j, \end{cases}$$

where the operator $(\ )_{j,\zeta}$ in the expressions above denotes differentiation with respect to the ζ of jth comparison function. In order to obtain a set of $4n$ first-order differentiation equations, we can define the state vector as

$$Z = \begin{Bmatrix} \chi \\ \dot{\chi} \\ \ddot{\chi} \\ \dddot{\chi} \end{Bmatrix}, \quad \dot{Z} = \begin{Bmatrix} \dot{\chi} \\ \ddot{\chi} \\ \dddot{\chi} \\ \ddddot{\chi} \end{Bmatrix}. \tag{30}$$

Substituting Eq. (30) into Eq. (29) yields

$$\begin{Bmatrix} \dot{\chi} \\ \ddot{\chi} \\ \dddot{\chi} \\ \ddddot{\chi} \end{Bmatrix} = \begin{bmatrix} \bar{0} & \bar{I} & \bar{0} & \bar{0} \\ \bar{0} & \bar{0} & \bar{I} & \bar{0} \\ \bar{0} & \bar{0} & \bar{0} & \bar{I} \\ -\bar{A}^{-1}\bar{E} & -\bar{A}^{-1}\bar{D} & -\bar{A}^{-1}\bar{C} & -\bar{A}^{-1}\bar{B} \end{bmatrix} \begin{Bmatrix} \chi \\ \dot{\chi} \\ \ddot{\chi} \\ \dddot{\chi} \end{Bmatrix} \Xi \tag{31}$$

Or Eq. (31) can be compactly rewritten in matrix form

$$\dot{Z} = HZ. \tag{32}$$

In Eq. (31), $\bar{0}$ is zero matrix and $\bar{I}$ is the identity matrix of size $n \times n$. It is an eigenvalue problem and μ represents the eigenvalues of matrix H. For non-trivial solutions, the characteristic equation is

$$\det|H - \mu\bar{I}| = 0. \tag{33}$$

The values of μ are complex eigenvalues that comprise real parts of τ's and imaginary parts of ω's, i.e., $\mu = \tau + \mathrm{i}\omega$. Note that the imaginary parts of ω's are transverse natural frequencies of the drill shaft.

The solution for the Euler–Bernoulli beam model of a spinning drill shaft containing flowing fluid and loaded by a compressive axial force can be easily found in a similar way.

4. Simulation results

The theoretical equations of motion based on the floating coordinate system derived in the preceding section were numerically simulated using MATLAB software. Drill shaft parameters and

material properties for these numerical simulations are listed in Appendix B. In the computer program, the assumed mode number n in Section 3 was set to 40 for convergence using Galerkin's method. The Timoshenko beam and Euler–Bernoulli beam models formulated in Eqs. (20) and (23) were studied under various drilling conditions such as different spinning speeds (Ω), compressive axial forces (P), and fluid flow velocities (U). The complex eigenvalues of the dynamic system were calculated using the characteristic Eq. (33). The transverse natural frequencies of the drill shaft were determined from the imaginary parts of the complex eigenvalues μ. The theoretical results for the Timoshenko beam and Euler–Bernoulli beam models were compared with each other.

The following dimensionless parameters were defined for the sake of clear representation: (a) $\bar{\omega} = \omega_n/\omega_{10}$, nth-mode non-dimensional natural frequency parameter; (b) $\bar{\Im} = \Omega/\omega_{10}$, non-dimensional spinning speed parameter; (c) $\bar{\Gamma} = U/U_{cr}$, non-dimensional fluid flow velocity parameter along the axial direction; (d) $\bar{\Re} = P/P_{cr}$, non-dimensional compressive axial force parameter. ω_{10} is natural frequency of the first mode of a non-spinning drill shaft without fluid. U_{cr} is the maximum value in the range of fluid flow velocities that we were interested in. Here, we set U_{cr} to 32 m/s from Chang [23, 24]. P_{cr} is the Euler critical buckling load given by $\pi^2 EI/l^2$.

Variations in natural frequencies corresponding to the first four mode-shapes of drill shaft at the dimensionless spinning speed parameter $\bar{\Im}$ are sketched in Figs. 3 and 4 for the clamped-hinged Timoshenko beam model described in Eq. (20). It can be seen that the static cutting fluid contained in BTA deep-hole drill tube decrease the transverse natural frequencies, and also that a natural frequency bifurcation occurred. There were four natural frequencies in each mode for the Timoshenko beam model. One pair of natural frequencies occurred at lower-orders of magnitude, the other at higher-orders of magnitude. Since the pair of natural frequencies occurring at higher orders of magnitude were of little significance, we considered only the pair of natural frequencies occurring at lower orders. There was only one pair of natural frequencies at lower-orders of magnitude for the Euler–Bernoulli beam model. It should be noted that if spinning ceases, only one

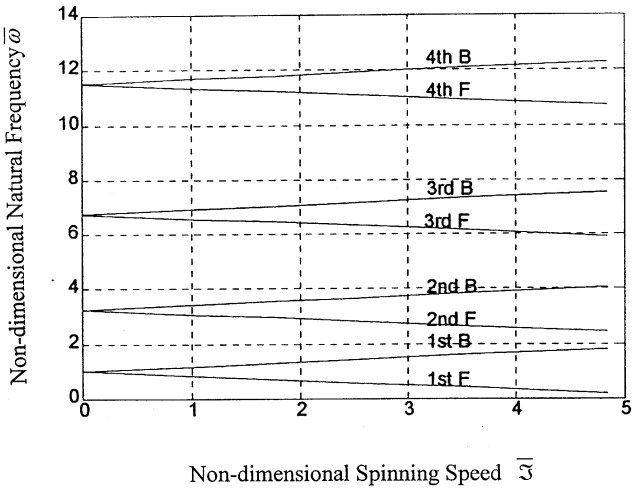

Fig. 3. Variations in natural frequency with spinning speed; without static fluid, $P = 0$ kg (F: forward precession B: backward precession).

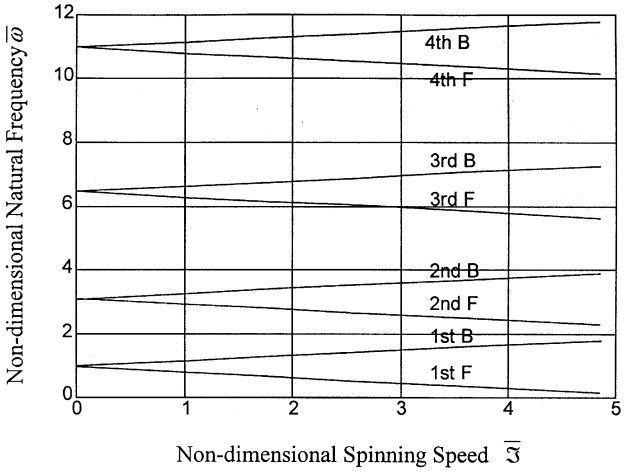

Fig. 4. Variations in natural frequency with spinning speed; with static fluid, $P = 0$ kg (F: forward precession B: backward precession).

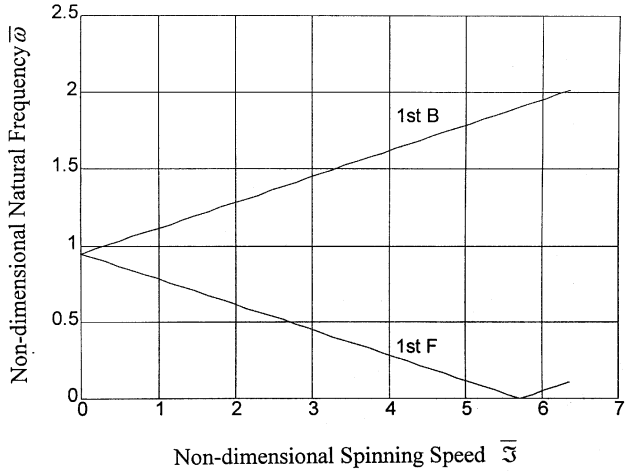

Fig. 5. Variations in the first natural frequency with spinning speed; with static fluid, $P = 0$ kg (F: forward precession B: backward precession).

natural frequency instead of two natural frequencies remains for each mode. The additional natural frequency is the bifurcation induced by Coriolis effects. In Figs. 3 and 4, the lower branches correspond to forward precession of the natural frequencies and the upper branches correspond to backward precession of the natural frequencies. This distinction between forward and backward precessions becomes more obvious at higher spinning speeds. The forward natural frequency decreases with increased spinning speed. When the forward natural frequency of the first mode decreased to zero, instability of the drill shaft occurred, see Fig. 5. The natural frequencies of the first four modes predicted by Timoshenko beam theory and Euler–Bernoulli beam theory are

plotted in Fig. 6. It can be seen that the two generated very close results for smaller drilling diameters. Slight differences occurred the lower modes at higher spinning speeds, but the difference in natural frequency between the two models became larger for the T-Max (drilling diameter greater than 65 mm) type deep-hole drill shaft.

The influence of fluid flow velocity on the first natural frequency, with no spinning speed and compressive axial force, is shown in Fig. 7. It can be observed that the natural frequencies depend heavily on fluid flow velocity. Fluid flow velocity tends to lower the transverse natural frequencies

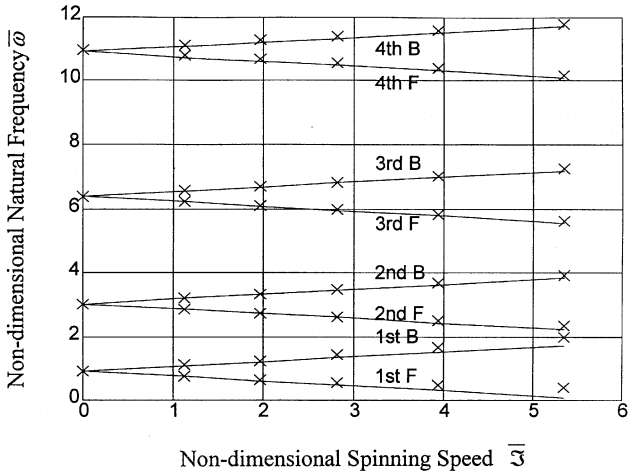

Fig. 6. Variations in natural frequency with spinning speed; with static fluid, $P = 0$ kg (F: forward precession B: backward precession) (–) Timoshenko beam, ($\times$) Euler–Bernoulli beam).

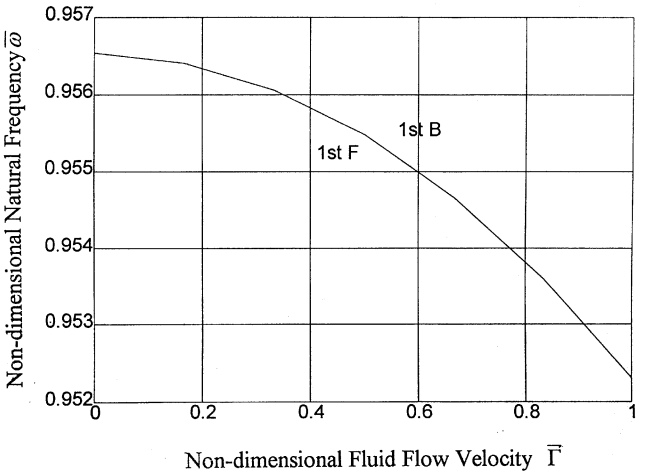

Fig. 7. Variations in the first natural frequency with velocity of flowing fluid; $P = 0$ kg, $\Omega = 0$ rpm, (F: forward precession B: backward precession).

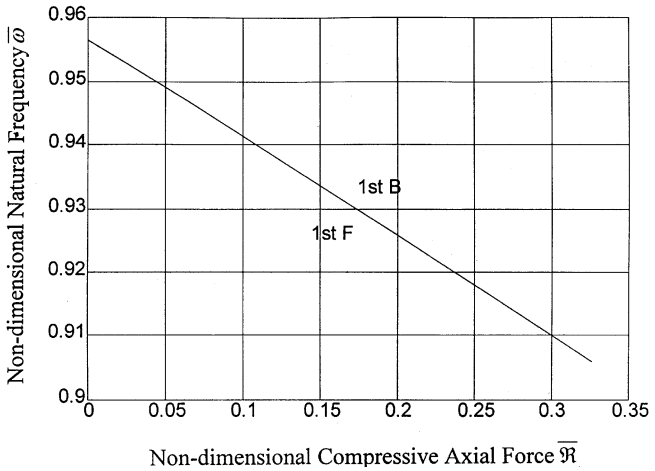

Fig. 8. Variations in the first natural frequency with compressive axial force; with static fluid, $\Omega = 0$ rpm, (F: forward precession B: backward precession).

Table 2
The natural frequencies of modes 1–4 of transverse vibration of a BTA drill shaft; without fluid; spinning speed $\Omega = 0$ rpm (unit: Hz)

Mode	0 kg	20 kg	40 kg	60 kg	80 kg	100 kg
ω_1	30.809	30.490	30.168	29.842	29.512	29.177
ω_2	99.743	99.279	98.813	98.345	97.874	97.400
ω_3	207.759	207.239	206.717	206.195	205.670	205.144
ω_4	354.452	353.901	353.350	352.797	352.243	351.689

of spinning drill shafts, especially, for the first natural mode, at which the effect of fluid flow velocity will result in instability in BTA deep-hole drilling as the critical flow velocity U_c is approached, i.e., the forward precession of natural frequencies decreases to zero.

The influence of compressive axial loads on the first natural frequency of a drill shaft with static fluid is plotted in Fig. 8. Variations in the first–fourth natural frequencies under compressive axial loading are listed in Tables 2–4. Compressive axial force applied to drill shafts tends to lower natural frequencies because the compressive axial forces soften the effective shaft stiffnesses. By contrast, the tensile force strengthens the effective shaft stiffness for higher-order vibration mode, decreasing the importance of this effect. Thus, we were concerned with lower-order vibration modes. In particular, the critical axial loading N_C results in instability as forward precession of the first natural frequency decreases to zero. This effect is similar to that of spinning speeds and fluid flow velocities in BTA deep-hole drill shaft. Results for both models for the first to fourth average natural frequencies of the drill shafts with and without static fluid, and spinning speed at 300 rpm

Table 3
The natural frequencies of modes 1–4 of transverse vibration of a BTA drill shaft; with static fluid; compressive axial force $P = 0$ kg (unit: Hz)

	Spinning speeds						
Mode	0 rpm	75 rpm	300 rpm	450 rpm	675 rpm	1050 rpm	1425 rpm
ω_1	31.250	30.950	30.500	30.250	30.000	29.300	29.000
ω_2	98.750	95.250	95.000	95.000	95.000	93.750	93.750
ω_3	202.750	191.500	190.000	190.000	190.000	189.000	190.000
ω_4	325.000	307.500	311.250	307.500	306.250	305.000	303.750

Table 4
The natural frequencies of modes 1–4 of transverse vibration of a BTA drill shaft; without fluid; compressive axial force $P = 0$ kg (unit: Hz)

	Spinning speeds					
Mode	0 rpm	300 rpm	525 rpm	750 rpm	1050 rpm	1425 rpm
ω_1	32.450	31.577	31.250	31.250	31.250	31.250
ω_2	102.500	97.745	97.500	97.500	96.250	93.750
ω_3	208.496	206.386	205.625	205.000	205.000	203.750
ω_4	345.514	333.372	332.500	332.500	332.500	331.250

Table 5
The natural frequencies of modes 1–4 of transverse vibration of a BTA drill shaft; with static fluid; compressive axial force $P = 0$ kg; spinning speed $\Omega = 300$ rpm (unit: Hz)

Mode	Experiment	Timoshenko	Euler
ω_1	30.500	29.470	29.477
ω_2	95.000	95.408	95.526
ω_3	190.000	198.734	199.307
ω_4	311.250	339.062	340.827

under zero compressive axial force are listed in Tables 5 and 6. Agreement was obtained for smaller drill shaft in this study. But for T-Max (above 65 mm) type deep-hole drill shafts, the effects of shear deformation, rotatory inertia moment, and gyroscopic moment could not be ignored. The difference in natural frequency between the two models was about 10% for 75 mm diameter drill shafts in numerical simulations.

Table 6
The natural frequencies of modes 1–4 of transverse vibration of a BTA drill shaft; without fluid; compressive axial force $P = 0$ kg; spinning speed $\Omega = 300$ rpm (unit: Hz)

Mode	Experiment	Timoshenko	Euler
ω_1	31.577	30.808	31.259
ω_2	97.745	99.742	100.004
ω_3	206.386	207.760	208.430
ω_4	333.372	354.452	356.354

5. Experiments

The experimental equipment used in this study is listed in Appendix B, and the experimental setups are shown schematically in Fig. 9. Impulsive and random-input-excitation tests were applied to non-spinning and spinning drill shafts to obtain the frequency responses from the dynamic systems. Test tool specifications are given in Appendix B.

Variations in the experimental first to fourth natural frequencies at various spinning speeds with and without flowing fluid are listed in Tables 3 and 4, respectively. The experimental and theoretical first to fourth natural frequencies of the spinning drill shaft with static fluid, no compressive axial force applied, and a spinning speed of 300 rpm are listed in Table 5. Similarly, the experimental and theoretical results for a spinning drill shaft without flowing fluid are listed in Table 6. We found that the experimental natural frequencies were in good agreement with the values predicted by our simulations.

6. Summary and conclusions

Two theoretical models of dynamic transverse vibrational behavior of spinning BTA deep-hole drill shafts were investigated on the basis of Timoshenko beam and Euler–Bernoulli beam theories, using formulations based on a floating coordinate system. Investigation of the Timoshenko beam model included considering the effects of shear deformation, rotatory inertia, gyroscopic moment, compressive axial force, and fluid flow velocity. The Euler–Bernoulli beam model of a spinning drill shaft is easily characterized using some simplifications of the equations for the Timoshenko beam model. The theoretical model presented here is closer to the complete physical tool shaft at high spinning speeds than the models established by Chin et al. [2] and Chin and Lee [1], who studied non-spinning simplified Euler–Bernoulli beam models.

Analyses of theoretical simulations and experimental investigations have been presented in this paper. The findings can be summarized as follows: (1) There are two sets of natural frequencies for each mode in the Timoshenko beam model, a higher order and a lower order of magnitude. There is only one set of a lower order of magnitude for the Euler–Bernoulli beam model. (2) The

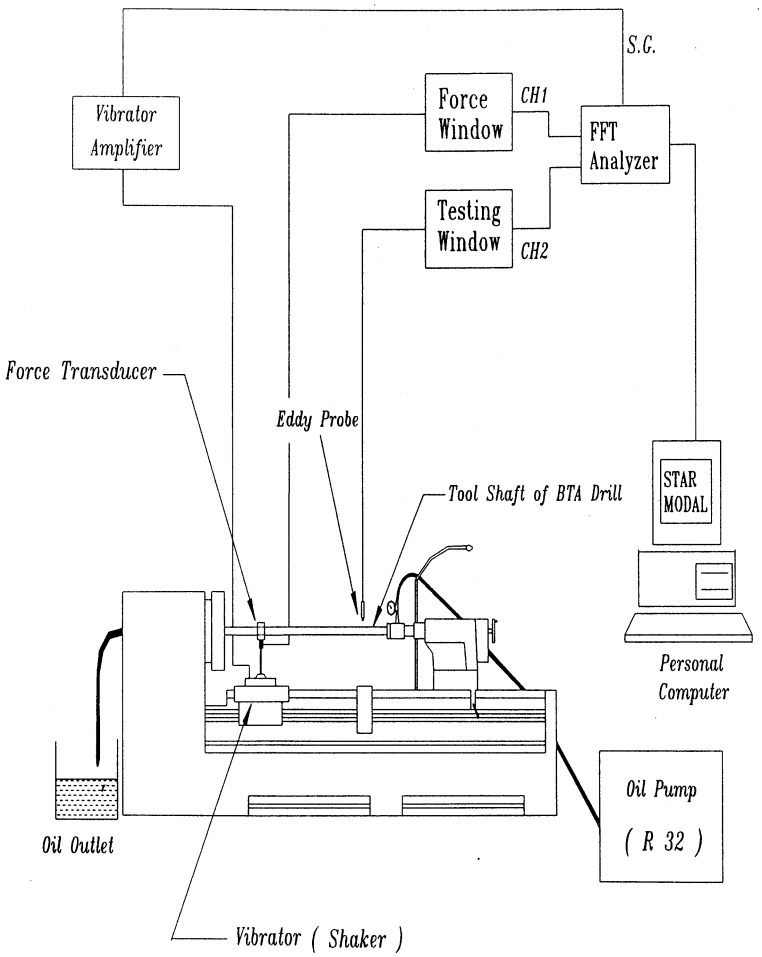

Fig. 9. Experimental setup for random-input testing.

Timoshenko beam and Euler–Bernoulli beam model display that the natural frequencies of the dynamic system possess backward and forward precession natural frequencies which depend strongly on spinning speeds. When spinning ceases, only one instead of two natural frequencies remain. The additional natural frequency is a bifurcation induced by Coriolis effects. (3) The distinction between backward and forward precessions becomes more obvious at higher spinning speeds. Since advances in bearing technology have made it possible to increase spindle speeds up to 60 000 rpm in high speed drilling, the effects of rotatory inertia and gyroscopic moments are significant when using BTA deep-hole drills. (4) The effect of fluid flow velocity tends to decrease transverse natural frequencies of spinning drill shafts. (5) Compressive axial force applied to spinning drill shafts softens the effective stiffness of the shafts, but the tensile force strengthens the effective stiffness of the shafts. The transverse natural frequency of a dynamic system decreases with applied force. (6) Theoretical simulations and experimental investigations showed good agreement.

Acknowledgements

The authors thank the National Science Council of the Republic of China for its support of this study under Grant Number NSC-86-2212-E-009-048.

Appendix A

From Fig. 2, the total slope of axis of a spinning drill shaft is equal to the sum of the slopes due to bending and shear angle.

$$\frac{\partial x}{\partial s} = \alpha + \gamma_1, \tag{A.1}$$

$$\frac{\partial y}{\partial s} = \beta + \gamma_2, \tag{A.2}$$

where α and β are rotational angles on the x_1–x_3 and x_2–x_3 planes, respectively. γ_1 and γ_2 are shear angles.

The axial displacement w of a point $(\bar{x}, \bar{y})$ from the centroidal line of the cross section can be expressed as

$$w = -\bar{x}\alpha - \bar{y}\beta. \tag{A.3}$$

The strain components of drill shafts are

$$\varepsilon_{11} = \varepsilon_{22} = 0, \tag{A.4}$$

$$\varepsilon_{33} = w_s = -\bar{x}\alpha_s - \bar{y}\beta_s, \tag{A.5}$$

$$\varepsilon_{23} = \tfrac{1}{2}(-\beta + y_s), \tag{A.6}$$

$$\varepsilon_{31} = \tfrac{1}{2}(-\alpha + x_s). \tag{A.7}$$

The stress components of drill shafts are

$$\sigma_{11} = \sigma_{22} = 0, \tag{A.8}$$

$$\sigma_{33} = E\varepsilon_{33} = -E\bar{x}\alpha_s - E\bar{y}\beta_s, \tag{A.9}$$

$$\sigma_{23} = 2G\varepsilon_{23}, \tag{A.10}$$

$$\sigma_{31} = 2G\varepsilon_{31}, \tag{A.11}$$

where E and G are Young's modulus and the shear modulus, respectively. In Timoshenko beam theory, shear coefficient k is introduced in the shear–stress equation as a correction factor [25] dependent on cross-sectional geometry. Therefore, shear–stress equations are given by

$$\sigma_{23} = 2kG\varepsilon_{23}, \tag{A.12}$$

$$\sigma_{31} = 2kG\varepsilon_{31}. \tag{A.13}$$

The strain energy is

$$V = \frac{1}{2}\int_v \sigma_{ij}\varepsilon_{ij}\,\mathrm{d}v \tag{A.14}$$

Appendix B

The experimental apparatus used:

1. Lathe: SAN SHING SK26120 heavy-duty precision lathe.
2. Deep-hole drill
   (a) Drill head (SANDVIK 420.6-0014D 18.91 70):
   Mass: 0.030205 kg
   Mass moment of inertia J: 1.420×10^{-6} kg m^2
   (b) Drill shaft (SANDVIK 420.5-800-2):
   Length: 1.6 m
   Internal diameter: 11.5 mm
   External diameter: 17 mm
   Material: JIS SNCM 21
   Density ρ: 7860 kg/m^3
   Young's modulus E: 206×10^9 pa
   Shear modulus G: 81×10^9 pa
   (c) Cutting fluid (R32):
   Densityρ_f: 871 kg/m^3
   Absolute viscosity: 0.383 kg/m s
3. Impulsive testing apparatus
   (a) Hammer (PCB 086 C03 SN7627):
   Range: 0-500 lb
   Amplifier: PCB model 480D06 power unit
   (b) Accelerometer (TEAC 601Z):
   Weight: 0.3 g
   Amplifier: TEAC SA620
   (c) Spectrum Analyzer: Signal doctor (PW-145C):
   Frequency range: 20–20 kHz
   Channel number: 2
   (d) Structural measuring system: STAR MODAL
4. Random-input testing apparatus:
   (a) Spectrum analyzer: same as that for impulsive testing
   (b) Structural measuring system: same as that for impulsive testing
   (c) Vibrator (LDS V203):
   Maximum sine force peak: 26.7 N (6.0 lb)
   Armature resonance frequency: 13 kHz
   Useful frequency range: 5–13000 Hz
   Amplifier: PW-PA100

(d) Force transducer (PCB 208 B01 SN 12904):
Calibration range: 0–10 lb
Sensitivity: 497.8 mV/lb
Linearity error: less than 1.0%
Resonance frequency: 70 kHz
(e) Eddy current probe (WS-2000):
Frequency range: 0–10 kHz
Gap range: 10–80 mils (1 mil $= 25.4 \times 10^{-3}$ mm)
Sensitivity: 200 mV/mil
Linearity error: $\pm$ 4%
Power supply: PW PS401, 24 V dc, 16 mA (MAX).

References

[1] Chin JH, Lee LW. A study on the tool eigenproperties of a BTA deep hole drill—theory and experiments. International Journal of Machine Tools Manufacture, Research and Application 1995;35(1):29–49.
[2] Chin JH, Hsieh CT, Lee LW. The shaft behavior of BTA deep hole drilling tool. International Journal of Mechanical Sciences 1996;38(5):461–82.
[3] Chin JH, Wu JS, Young RS. The computer simulation and experimental analysis of chip monitoring for deep hole drilling. ASME Journal of Engineering for Industry 1993;115:184–92.
[4] Chin JH, Wu JS. Mathematical models and experiments for chip signals of single-edge deep hole drilling. International Journal of Machine Tools Manufacture, Research and Application 1993;33(3):507–19.
[5] Chin JH, Lin SA. Dynamic modelling and analysis of deep-hole drilling process. International Journal of Modelling and Simulation 1996;16(3):157–65.
[6] Sakuma K, Taguchi K, Katsuki A. Study on deep-hole boring by BTA system solid boring tool—behavior of tool and its effects on profile of machined hole. Bulletin of the Japan Society of Precision Engineering 1980;14(3):143–8.
[7] Huang TC. The effect of rotatory inertia and of shear deformation on the frequency and normal mode equations of uniform beams with simple end conditions. ASME Journal Applied Mechanics 1961:579–84.
[8] Zu JWZ, Han RPS. Natural frequencies and normal modes of a spinning Timoshenko Beam with general boundary conditions. ASME Journal of Applied Mechanics 1992;59:197–204.
[9] Eshleman RL, Eubanks RA. On the critical speed of a continuous rotor. ASME Journal of Engineering for Industry 1969;1180–8.
[10] Nelson HD. A finite rotating shaft element using Timoshenko beam theory. ASME Journal of Mechanical Design 1980;102:793–803.
[11] Bauer HF. Vibration of a rotating uniform beam, part I: orientation in the axis of rotation Journal of Sound and Vibration 1980;72(2):177–89.
[12] Lee CW, Katz R, Ulsoy AG, Scott RA. Modal analysis of a distributed parameter rotating shaft. Journal of Sound and Vibration 1988;122(1):119–30.
[13] Sato K. On the governing equations for vibration and stability of a Timoshenko beam: Hamilton's principle. Journal of Sound and Vibration 1991;145(2):338–40.
[14] Choi SH, Pierre C, Ulsoy AG. Consistent modeling of rotating Timoshenko shafts subject to axial loads. ASME Journal of Vibration and Acoustics 1992;114:249–59.
[15] Farchaly SH, Shebl MG. Exact frequency and mode shape formulate for studying vibration and stability of Timoshenko beam system. Journal of Sound and Vibration 1995;180(2):205–27.
[16] Housner GW, Calif P. Bending vibrations of a pipe line containing flowing fluid. ASME Journal of Applied Mechanics 1952:205–8.
[17] Paidoussis MP. Dynamics of tubular cantilevers conveying fluid. International Journal of Mechanical Engineering Sciences 1970;12(2):85–103.

[18] Paidoussis MP, Issid NT. Dynamic stability of pipes conveying fluid. Journal of Sound and Vibration 1974;33(3): 267–94.
[19] Weaver DS, Unny TE. On the dynamic stability of fluid-conveying pipes. ASME Journal of Applied Mechanics 1973:48–52.
[20] Blevins RD. Flow-induced vibration, Chap. 10, New York: Krieger Publication, 1986.
[21] Han RPS, Zu JWZ. Modal analysis of rotating shafts: a body-fixed axis formulation approach. Journal of Sound and Vibration 1992;156(1):1–16.
[22] Katz R, Lee CW, Ulsoy AG, Scott RA. The dynamic response of a rotating shaft subject to a moving load. Journal of Sound and Vibration 1988;122(1):131–48.
[23] Chang SG. An investigation into torsional behavior of BTA deep hole drill shaft and the effects of fluid speed. Master thesis, National Chiao Tung University, Taiwan, ROC 1995, 59–61.
[24] Catalog. Rotating Tools, C-1100:4-ENG SANDVIK Coromant, 1995.
[25] Cowper GR. The shear coefficient in Timoshenko's beam theory. ASME Journal of Applied Mechanics 1966:335–40.